




Stabilization of a Harmonic Mode-Locking by Shifting the Carrier Frequency

Dmitry A. Korobko , Dmitrii A. Stoliarov , Pavel A. Itrin, Valeria A. Ribenek, Maxim A. Odnoblyudov, Andrei B. Petrov, and Regina V. Gumenyuk , *Member, IEEE*

Abstract—Harmonically mode-locked soliton fiber lasers have been intensively investigated in recent years due to their wide range of applications. Drawback of these lasers is relatively large timing jitter which is significantly higher than the timing jitter in lasers operating at fundamental frequency. We report the stabilizing frequency shift effect in harmonic mode-locking ring soliton fiber laser that is studied theoretically and numerically. It is known that a harmonic mode-locking regime in a fiber laser occurs due to interpulse repulsion, which leads to a uniform distribution of pulses in the cavity. We demonstrate that the frequency shift contributes to an increase in the hardness of interpulse interactions and can lead to stabilization of the periodic arrangement of pulses. The experiment carried out confirms the theoretical predictions and the results of numerical simulation.

Index Terms—Fiber lasers, laser mode-locking, timing jitter.

I. INTRODUCTION

ASER sources of pulse trains with a high repetition rate commonly employed in a wide list of applications in spectroscopy, telecommunications, microwave photonics [1]–[3]. Soliton fiber lasers with passive harmonic mode-locking (HML) represent as one of the most promising alternatives of such

lasers sources [4]–[6]. Besides that, exhibiting advantageous consumer properties, such as compactness, reliability, low cost and convenience of beam delivery approach these sources are among the most attractive alternatives for material processing, medicine lasers and other areas [7], [8]. Since HML fiber lasers are complex systems, there are several approaches for their classification based on different criteria. The most obvious one is by a mode-locking technique, e.g., by using nonlinear polarization rotation (NPR) [9], [10] or special saturable absorbers based on carbon nanotubes or graphene [11], [12]. Another classification method is related to a mechanism of the HML implementation in the cavity; here two large groups of fiber lasers can be specified. In the first group the HML occurs due to special intra-cavity periodic filter with a free spectral range (FSR) which is a multiple of the main cavity FSR and equals to the pulse repetition rate [13]. In this case, a quite high Q-factor of the filter is essential to generate multi-GHz pulse train allowing selection of individual modes from thousands of modes of the main cavity [14], [15]. The second group of HML lasers in this classification is attractive for the scientific community due to the automatic arrangement of strongly periodic pulse pattern in the laser cavity through pulse repulsion [16]. However, it is difficult to specify the mechanism of pulse repulsion for each case. It can be based on interaction through saturating and relaxing dissipative parameters [1], [17], continuous-wave (CW) radiation component, dispersion waves [18], or acoustic waves induced by electrostriction [19], etc. A common feature of all interaction induced effects is low intensity, in many cases only slightly exceeding the noise level (associated, for example, with noise in the active medium, thermal effects, vibrations, etc.). The noise-induced fluctuations in the time interval of the HML pulse train are known as HML timing jitter, and its value is significantly higher than the timing jitter in lasers operating at fundamental frequency [20]. It is a major drawback of the HML laser technology. The timing jitter suppression and improvement of the pulse train stability will essentially increase the HML lasers attractiveness, in particular, for such highly demanding application as frequency comb generation. Intuitively, the simplest way to suppress temporal jitter in HML fiber lasers and stabilize the pulse position is to enhance the pulse repulsion by deepening the “potential wells” in which pulses are located. Although, a direct implementation of this method is hardly possible.

Recently, a series of experimental works revealed that employment of intracavity frequency shift increased the stability of the HML in fiber lasers [21]–[23]. In such laser, the radiation

Manuscript received October 22, 2020; revised January 23, 2021 and March 1, 2021; accepted March 22, 2021. Date of publication March 29, 2021; date of current version May 2, 2021. This work was supported by the Russian Science Foundation under Grant 19-72-10037 and the Russian Ministry of Higher Education and Science (Megagrant Program, project #2020-220-08-1369). The work of Regina V. Gumenyuk was supported by the Academy of Finland Flagship Programme, Photonics Research and Innovation (PREIN) under Grant 320165. The work of Maxim A. Odnoblyudov and Andrei B. Petrov was supported by the Russian Ministry of Science and Higher Education as part of World-class Research Center program: Advanced Digital Technologies under Grant #075-15-2020-934. (*Corresponding author: Dmitry A. Korobko.*)

Dmitry A. Korobko, Pavel A. Itrin, and Valeria A. Ribenek are with Ulyanovsk State University, 432017 Ulyanovsk, Russia (e-mail: korobkotam@rambler.ru; itrin@mail.ru; ribl98@mail.ru).

Dmitrii A. Stoliarov is with Ulyanovsk State University, 432017 Ulyanovsk, Russia, and also with Aston University, B4 7ET, Birmingham, U.K. (e-mail: dmitreyst@gmail.com).

Maxim A. Odnoblyudov is with Peter the Great St. Petersburg Polytechnical University, 195251 St. Petersburg, Russia (e-mail: maxim.odnoblyudov@spbstu.ru).

Andrei B. Petrov is with Peter the Great St. Petersburg Polytechnical University, 195251 St. Petersburg, Russia, and also with the Saint-Petersburg National Research University of Information Technologies, Mechanics and Optics, 197101 St. Petersburg, Russia (e-mail: 79602507133@yandex.ru).

Regina V. Gumenyuk is with Ulyanovsk State University, 432017 Ulyanovsk, Russia, and also with the Laboratory of Photonics, Tampere University of Technology, 33720 Tampere, Finland (e-mail: regina.gumenyuk@tuni.fi).

Color versions of one or more figures in this article are available at <https://doi.org/10.1109/JLT.2021.3068822>.

Digital Object Identifier 10.1109/JLT.2021.3068822

frequency is determined by a balance between the shift introduced by an acousto-optical modulator (AOM) and the opposite nonlinear frequency shift induced by a spectral filter and depended on radiation bandwidth [24], [25]. This effect underlies the so-called frequency shifting feedback (FSF) mode-locking mechanism, which is based on a soliton pulse separation from a narrow-band continuum [26], [27]. Introducing the frequency shift in the pattern of interacting pulses causes the breaks of the system symmetry leading to a change in the hardness of the pulse interaction [22]. The present study is aimed to discover the physical basis of this effect and to demonstrate theoretically and experimentally the enhanced stability of HML in soliton fiber lasers with the FSF mechanism.

II. THEORETICAL FRAMEWORK

In this section, we underly the theoretical basis of an HML stabilization in a soliton fiber laser with an intracavity frequency shift. The theory assumes that the effects of NPR and other intensity-dependent losses responsible for mode-locking except frequency shift can be neglected. These mode-locking mechanisms can be considered as small stabilizing perturbations and do not strongly affect the main question concerning the collective pulse dynamics.

We use the following notations for the parameters of the considered model: β_{2r} , γ_r are the group velocity dispersion (GVD) and coefficient of Kerr nonlinearity of the cavity correspondingly, g , l are the gain and losses per round trip, Ω_f is the width of spectral filter. We also introduce the dimensionless propagation length $z_r = z/L_r$, which is a multiple of the cavity length, and characteristic time τ_0 , which we choose so that the values of the parameters can be effectively averaged over the dispersion length $Z_D = \tau_0^2/\beta_{2r}$. Pulse propagation in a ring laser in the presence of a frequency shift and filter is described by the averaged nonlinear Schrödinger equation (NLSe) with perturbation. In soliton units, it can be written as follows [25]:

$$\frac{\partial u}{\partial Z} - \frac{i}{2} \frac{\partial^2 u}{\partial \tau^2} - i|u|^2 u = \delta u + \beta \left(\frac{\partial}{\partial \tau} + i\omega_{AOM} \right) u, \quad (1)$$

where $\delta = (g - l)Z_d$ is the parameter of excess (exceeding loss) gain, $\beta = 2/(|\beta_{2r}|\Omega_f^2)$ is the filter dispersion and $\dot{\omega}_{AOM} = 2\pi\Delta\nu t_0^3/\beta_{2r}$ is the dimensionless frequency shift rate ($\Delta\nu$ is the frequency shift of the AOM in Hz). The one-soliton solution of the non-perturbed NLSe with $\delta = \beta = 0$ reads as

$$u_1(Z, \tau) = \eta_1 \operatorname{sech}(\eta_1(\tau - \tau_1(Z))) \exp(i\omega_1(Z)\tau + i\phi_1(Z)),$$

$$\omega_1 = \partial\tau_1/\partial Z, \partial\phi_1/\partial Z = (\eta_1^2 - \omega_1^2)/2, \quad (2)$$

where η_1 , τ_1 , ω_1 and ϕ_1 are the amplitude, coordinate, frequency and the phase of the pulse, respectively. It should also be noted that the soliton velocity is determined by its frequency ω_1 . Using the standard approach of perturbation theory, one obtains the equations describing the pulse frequency and amplitude changing under the influence of the right-hand side of the Eq. (1) [25]:

$$\partial\omega_1/\partial Z = \dot{\omega}_{AOM} - 4\beta\eta_1^2\omega_1/3,$$

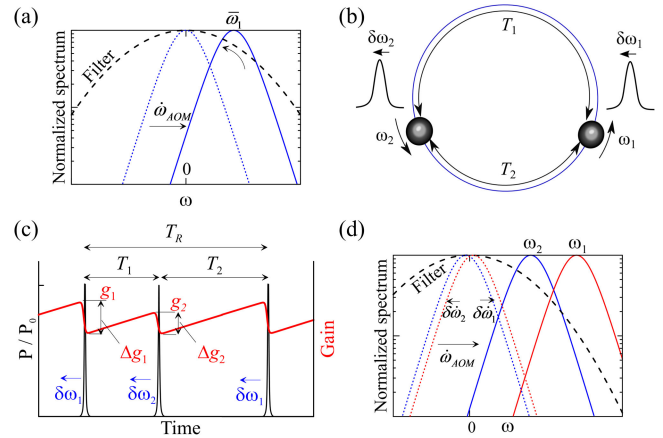


Fig. 1. (a) Normalized soliton spectrum under the action of frequency shift $\dot{\omega}_{AOM}$. The dotted line denotes the soliton spectrum in the absence of the shift. (b) Scheme of interaction of two pulses in a ring cavity with a fundamental period T_R . T_1, T_2 are the temporal distances between pulses, where $T_1 + T_2 = T_R$. $\delta\omega_1, \delta\omega_2$ are the changes in the frequency of one pulse under the influence of another, corresponding to the values of velocity drifts. (c) The scheme of interaction of two pulses through the gain depletion and recovery. The values of velocity drifts are proportional to the gain jumps $\delta\omega_i \propto \Delta g_i$. (d) Normalized spectra of solitons interacting through GDR with the frequency shift introduced by $\dot{\omega}_{AOM}$. The dotted lines denote the soliton spectra in the absence of a shift.

$$\partial\eta_1/\partial Z = 2\delta\eta_1 - 2\beta\eta_1(\eta_1^2/3 + \omega_1^2). \quad (3)$$

When a frequency shift does not exceed the critical value $\dot{\omega}_{AOM} < \Delta\omega_0 = 8\delta\sqrt{\delta}/8\beta\sqrt{3\beta}$, the soliton is trapped by the filter and its frequency and amplitude tend to some stationary values $(\bar{\omega}_1, \bar{\eta}_1)$. At these values the frequency shift is balanced by the return shift induced by the spectral filter, which increases with the filter slope (Fig. 1(a)). At a stationary point, the relation $\bar{\omega}_1 = 3\dot{\omega}_{AOM}/4\beta\eta_1^2$ is fulfilled, so a soliton of smaller amplitude with narrower spectrum moves further from the center of the filter $\omega = 0$. This effect, in particular, is associated with the soliton frequency shifting feedback (FSF) mode-locking [25]–[27], which ensures the separation of solitons from narrow-band low-intensity radiation.

Further, we will continue our consideration by taking into account the effects of the pulse interaction and using an example of two pulses in a ring cavity with a fundamental period T_R . Schematically, this interaction is similar to the interaction of two small objects separated by time distances T_1, T_2 ($T_1 + T_2 = T_R$) and moving in a circle (Fig. 1(b)). The interaction can be caused by dispersive [28] or acoustic [19] waves excited by the pulses, changes of dissipative parameters [17], [29] etc. Under the action of one of the pulses, the velocity of another pulse gets incremental change by the value $\delta\omega_i$ and vice versa, so the relative velocity of the pulses changes by $(\delta\omega_1 - \delta\omega_2)$. The strength of the pulse interaction depends on the temporal inter-pulse distances. If condition $T_1 < T_2$ implies $(\delta\omega_1 - \delta\omega_2) > 0$, then the faster pulse “runs away” which leads to equalization of the inter-pulse distances and harmonic mode-locking. This case corresponds to the pulse repulsion. In the inverse scenario, the same condition $T_1 < T_2$ leads to the attraction of pulses $(\delta\omega_1 - \delta\omega_2) < 0$, when the slow pulse is “caught up” with the faster one.

The method of the HML stabilization by the frequency shift as a supporting mechanism is applicable for any type of pulse repulsion. In more detail we will consider the simplest and most demonstrative kind of pulse interaction induced by gain depletion and recovery (GDR) (Fig. 1(c)) [29]. Qualitatively, within the process of depleting and recovering of the active medium population inversion, the pulse experiences a time-dependent gain, i.e., the leading edge of the pulse receives more gain than the trailing edge. This time-dependent gain generates a velocity drift of the pulse toward the region of higher gain (to the region $t \rightarrow -\infty$). The value of the velocity drift is proportional to the gain depletion $\delta\omega_i = a \Delta g_i$. A simple analysis shows that if initially $T_1 < T_2$, then $g_1 > g_2$ since the gain has more time to recover before the first pulse. Thus, it leads to $\Delta g_1 > \Delta g_2$, and as a result $\delta\omega_1 > \delta\omega_2$. The condition $T_1 > T_2$ in its turn implies $\delta\omega_1 < \delta\omega_2$, i.e., the pulse repulsion occurs anyway. Denoting τ_g as the gain relaxation time and $\alpha \gg 1$ as the proportionality coefficient in the relation $\Delta g_i = g_i/\alpha$, it can be shown that [29]:

$$\begin{aligned} \delta\omega_1 + \delta\omega_2 &= aT_R(T_1 + T_2)/\tau_g = aT_R^2/\tau_g = \text{const}, \\ \delta\omega_1 - \delta\omega_2 &= \frac{aT_R/\tau_g}{2\alpha - 1}(T_2 - T_1) = -A(T_1 - T_2), \quad A > 0, \end{aligned} \quad (4)$$

e.g., the average velocity of pulses is constant. Therefore, when one of the pulses slows down, another accelerates. It's important that equations for the pulse frequencies, which are fundamentally similar to the system (4), can be obtained for other types of pulse repulsion, for example, for pulses interacting through acoustic waves [19]. Taking into account that $(\delta\omega_1 - \delta\omega_2) = d(T_1 - T_2)/dZ$, we come to the limit $(T_1 - T_2) \rightarrow 0$, thus, we confirm that the repulsion through the GDR leads to the equalization of the interpulse distances and formation of the harmonic mode-locking. It should be noted that the gain relaxation time ($\tau_g \sim 10^{-4}$ s and even more for Er-doped fibers) significantly exceeds the laser's fundamental period $\tau_g \gg T_R$, so the speed of equalization of T_1 and T_2 determined by the value of A is relatively slow. This fact means the weakness of the interaction between pulses and its relatively low resistance to noise-induced fluctuations.

As the next step, we show that the strength of pulse interaction can be changed, when the frequency shift is applied to the system with the GDR induced effects. Considering a system without a shift, we assume that at the initial moment $T_1 > T_2$, thus velocity variations are $(\delta\omega_1 - \delta\omega_2) < 0$, and in a system associated with an average velocity, the first pulse slows down, and the second accelerates (Fig. 1b). Determining the acceleration as a change in the pulse velocity per unit length Z (the value corresponding to the left part of the first equation (3)) it can be found that it is proportional to the time interval difference $\Delta = (T_1 - T_2)$: $\delta\dot{\omega}_2 = -\delta\dot{\omega}_1 = B \cdot \Delta$, where the coefficient $B \sim A/l_r > 0$. So, in the system associated with an average velocity, the pulses experience small frequency drift in opposite directions $\delta\dot{\omega}_2 = -\delta\dot{\omega}_1$ (Fig. 1(d)). By superimposing on this a frequency shift $\dot{\omega}_{AOM}$ induced by the AOM, we see that the pulses possess the different frequency shifts of different magnitude $\dot{\omega}_{AOM} \pm \delta\dot{\omega}_1$. In the case when a frequency shift opposite to the average

velocity (corresponding to frequency up-shift), the equations (3) for each pulse are transformed into the form

$$\begin{aligned} \partial\omega_i/\partial Z &= \pm B\Delta + \dot{\omega}_{AOM} - 4\beta\eta_i^2\omega_i/3, \\ \partial\eta_i/\partial Z &= 2\delta\eta_i - 2\beta\eta_i(\eta_i^2/3 + \omega_i^2), \quad i = 1, 2. \end{aligned} \quad (5)$$

In the case of the frequency down-shift, the equations (5) can be written in the same form; however, to avoid negative frequencies the signs of the first term should be inverted $\mp B\Delta$. It is important to note that the form of the Eq. 5 is independent on the mechanism responsible for the pulse interaction in the cavity. If other than GDR is considered the form of the equations (5) will be same. Physically, a nonlinear system (5) shows how a frequency up-shift affects the characteristics of interacting pulses coupled through the Δ parameter. Combining Eqs. (5), we obtain the following system of equations that is similar to obtained in Ref. [25] in case of direct pulse interaction

$$\begin{aligned} \partial\eta/\partial Z &= 2\delta\eta - 2\beta\eta(\eta^2/3 + \omega^2), \\ \partial p/\partial Z &= 2p(\delta - \beta(\eta^2 + \omega^2)) - 4\beta\eta\omega q, \\ \partial\omega/\partial Z &= \dot{\omega}_{AOM} - 4\beta\eta^2\omega/3, \\ \partial q/\partial Z &= -B\Delta - 4\beta\eta^2q/3 - 8\beta\eta\omega p/3, \\ \partial\Delta/\partial Z &= -2q. \end{aligned} \quad (6)$$

Here $\eta = (\eta_1 + \eta_2)/2$ is the average amplitude, $p = (\eta_2 - \eta_1)/2$ is the amplitude differences, $\omega = (\omega_1 + \omega_2)/2$ is the average frequency and $q = (\omega_2 - \omega_1)/2$ is the frequency difference. The system of equations (6), which describes the dynamics of two interacting pulses under the influence of the frequency shift, has a stationary point ($\eta = \bar{\eta}$, $p = 0$, $\omega = \bar{\omega}$, $q = 0$, $\Delta = 0$) corresponding to pulses of equal amplitude and frequency, uniformly distributed over the cavity $T_1 = T_2$. We would like to note that the system of equations (6) can be generalized to an arbitrary number of pulses, sequentially separated by time distances τ_i , similarly shown in [29]. The evolution of the system to a stationary point with corresponding different initial conditions is shown in Fig. 2. The upper row (Fig. 2(a-c)) illustrates the equalization of the interpulse distances for two pulses with the same frequency initially non-periodically arranged in the cavity with $\Delta = (T_1 - T_2) = 5$. The main result is in the presence of frequency shift $\dot{\omega}_{AOM} \neq 0$ the system approaches to the equilibrium point much faster (Fig. 2(a)). Comparison of the phase trajectories shows that in the absence of the shift the system trajectory stays within the region of small frequency q and amplitude p variations (Fig. 2(b, c)). The frequency shift breaks the system symmetry and leads to an increase in these parameters in the transitional phase. As a result, the asymmetry in the pulse frequencies accelerates the changes in Δ (see the last equation of the system (6)), which is similar to an increase in the strength of interpulse repulsion.

A similar result is obtained for pulses uniformly distributed over the cavity $\Delta = 0$ at the starting point, but with different initial frequencies $q \neq 0$ (Fig. 2(d-f)). In this case, the deviation from the periodic pulse distribution is induced $\Delta \neq 0$ under a condition of the fast equalization of the pulse frequencies.

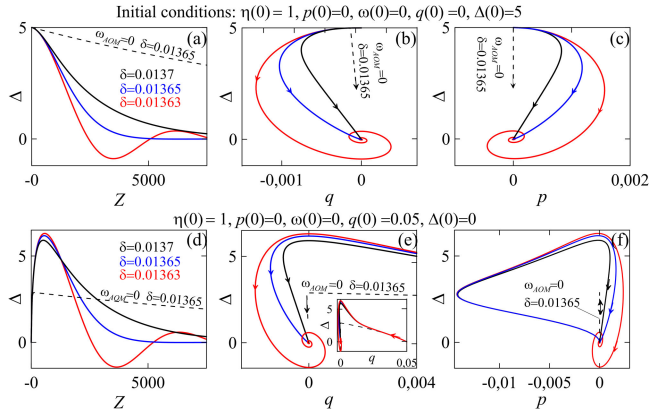


Fig. 2. Evolutionary trajectories of the system (6) with parameters $\beta = 0.015$, $\omega_{AOM} = 0.02$, $B = 1.5 \cdot 10^{-6}$ to a stationary point under the indicated initial conditions. (a), (d) – change of the interpulse distance Δ ; (b), (e) – phase trajectories in coordinates (q, Δ) ; (c), (f) – phase trajectories in coordinates (p, Δ) . Solid lines correspond to the indicated values of δ . The dashed line shows the trajectory of the system evolution in the absence of a frequency shift $\omega_{AOM} = 0$. Fig. (e) shows part of the phase trajectory in enlarged scale, the full trajectory is shown in the inset.

Further, the process develops completely similar to the previous one – the phase trajectories of the frequency-shifted system stay within the region of essentially nonzero values of the frequency q and amplitude p , which accelerates the achievement of the equilibrium point $\Delta = 0$. Also in both case in the presence of a frequency shift, the higher gain level contributes to the less pronounced asymmetry of the system, so the time requiring to approach the equilibrium point can be significantly reduced by choosing the optimal gain value δ . Returning to the mechanical analogy, we can say that the frequency up-shift from the center of the filter causes an increase in the hardness of the repulsion and stabilization of the periodical arrangement of the pulses in the cavity. We should note that the maximum achievable repetition rate is determined by the efficiency of interpulse interaction comparing to the noise level. In case of repulsion caused by GDR this efficiency can be quantified by the ratio of the interpulse spacing to the gain recovery timescale T_i/τ_g , that decreases with increasing pulse repetition rate. Thus, in real laser system increase in the repetition rate to the highest value is possible with the higher energy of an individual pulse while maintaining the noise characteristics at a fixed level, or with a radical reduction in noise (temperature stabilization, reduction of pump noise, etc). As for the frequency down-shift the analysis similar to carried out in this section shows that in this case the sign of the pulse interaction is inverse, thereby, resulting in the pulse attraction: $\Delta \rightarrow T_R$.

III. NUMERICAL SIMULATION

The theoretical analysis shows that the frequency up-shift from the center of the spectral filter is a promising approach for the HML stabilization in a fiber soliton laser. This conclusion will be further confirmed by the results of numerical simulations. The diagram of the laser model being under consideration is shown in Fig. 3. Briefly, the model operates as follows. A linearly polarized signal is amplified in the gain fiber at the same time being affected by depletion and recovery of the gain. Since the



Fig. 3. The scheme of a fiber ring laser used in the numerical simulation. SA – saturable absorber, OC – output coupler, SMF – single-mode fiber.

gain is time-dependent due to the GDR effect, the amplification level of the signal depends on its temporal profile. The signal then propagates in a standard SMF and passes through an element corresponding to an ideal fast saturable absorber. Before passing through the filter the signal frequency is up-shifted. Finally, after the experience of losses in the output coupler, the signal re-enters the gain fiber. The signal propagation in fiber elements is described by the NSE equation:

$$\frac{\partial A}{\partial z} - i\frac{\beta_2}{2}\frac{\partial^2 A}{\partial t^2} - i\gamma|A|^2A = \frac{g(t)A}{2}, \quad (7)$$

where $A(z, t)$ is the amplitude of the linearly-polarized wave, β_2 , γ are the values of the group velocity dispersion (GVD) and the Kerr nonlinearity of the fiber. Naturally, the signal propagating through the SMF meets zero gain $g = 0$. Since the filter included in the scheme is narrow band, it makes possible to consider the gain spectrally flat, while the time dependence of the gain (Fig. 1(c)) is described by the standard rate equation:

$$\frac{dg}{dt} = \frac{g_0 - g}{\tau_g} - \frac{g|A(z, t)|^2}{E_g}. \quad (8)$$

Here g_0 is the small-signal gain, E_g is the gain saturation energy and τ_g is the gain relaxation time. We would like to note that the present research is not aimed to study the internal evolution of laser mode-locking. Thus, to simplify the problem, the ideal saturable absorber is introduced by a transfer function $A'(t) = A(t)(1 - \alpha(t))$ with a response

$$\alpha = \frac{\alpha_0}{1 + |A(z, t)|^2/P_s}$$

is expressed in terms of its modulation depth α_0 and saturation power P_s . Physically, this element corresponds to the NPR mode-locking mechanism or any sufficiently fast saturable absorber. The frequency up-shift and filter are described by the transfer functions $A'(\Omega) = A(\Omega + 2\pi f)$, $A'(\Omega) = A(\Omega) \exp(-\Omega^2/2\Omega_f^2)$, where Ω_f is the Gaussian filter bandwidth. The output ratio of the coupler is 10%.

Two pulses with interpulse distances $T_1 \neq T_2$, $T_R = T_1 + T_2$ is settled as an initial condition. Periodic boundary conditions with window size $\tau_{win} = T_R$ consisting of 2^{12} points are used for simulation. The frequency shift is equal to the step of the frequency grid $2\pi f = d\Omega$. The main parameters of the model are specified in Table I. The length of the fiber elements is chosen as $l_g = 2.5$ m for the gain fiber and $l_{SMF} = 10$ m for SMF; thus the net cavity dispersion is $\beta_{2\Sigma} = -0.25$ ps². Note that for real lasers, the values of the parameters τ_g and T_R exceed the selected ones by a factor of thousands. It has been done to speed up the simulation. Nevertheless, the choice fully satisfies the necessary condition $T_R \ll \tau_g$ and is adequate to describe the interaction through the GDR. The main condition of the successful laser

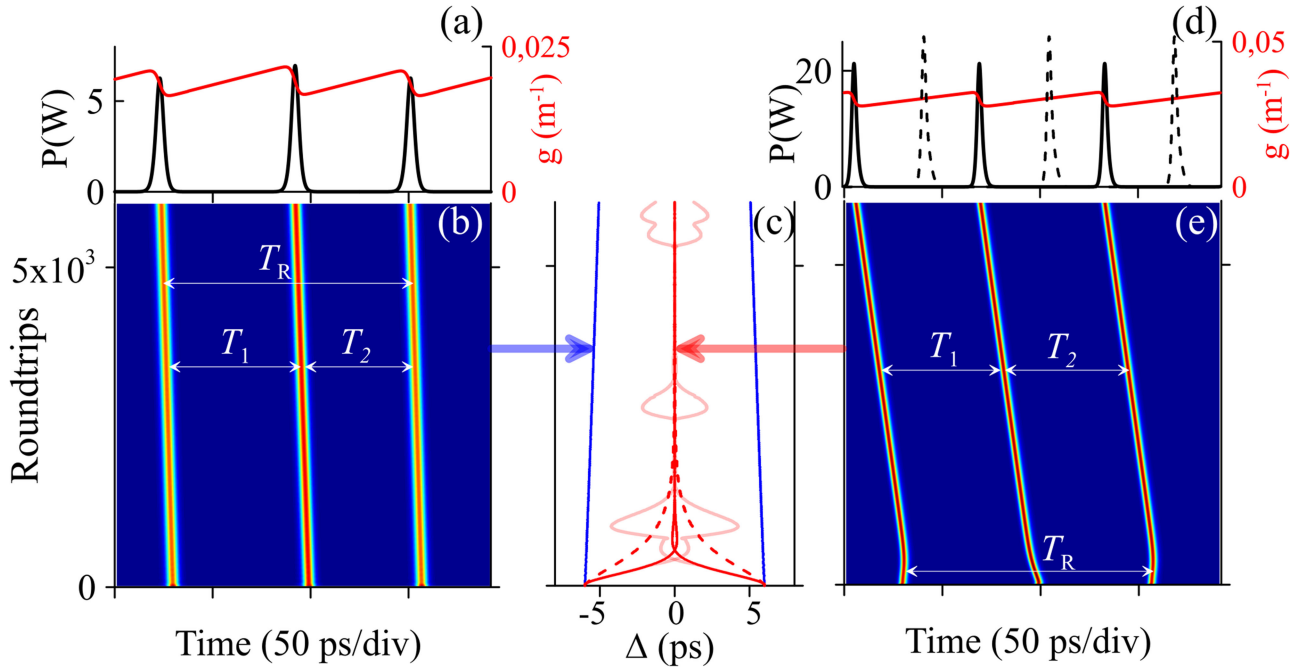


Fig. 4. (a), (b) Pulse propagation in the presence of a saturable absorber without frequency up-shift. (a) Pulse arrangement and gain $g(t)$ distribution after 6000 cavity roundtrips. (b) Pulse evolution diagram in the cavity. (c) Evolution of interpulse distance differences Δ and $-\Delta$ in the model with saturable absorber without the frequency up-shift (blue) and with frequency up-shift (red lines). The dashed red lines correspond to the scheme with frequency up-shift, but without saturable absorber. (d), (e) - same as (a), (b), but with frequency up-shift. For comparison, the dashed lines in (d) show pulse arrangement obtained in the scheme with frequency up-shift, but without saturable absorber. The changes Δ and $-\Delta$ in the presence of noise perturbations are shown by pale red lines.

TABLE I
THE PARAMETERS OF THE LASER USED IN THE SIMULATION

Parameter	Value	Parameter	Value
γ ($\text{W}^{-1} \text{m}^{-1}$)	0.0015	T_R (ps)	128
β_2 ($\text{ps}^2 \text{m}^{-1}$)	-0.02	τ_g (ns)	5
Ω_f (ps^{-1})	1.33 (FWHM ~ 3 nm at $\lambda \approx 1550$ nm)	α_0	0.05
g_0 (m^{-1})	0.9	P_s (W)	5

mode-locking is the positive feedback that occurs when the higher transmission of the cavity corresponds to the pulse with higher peak power [30], [31]. Such positive feedback executes suppression of low-intensity radiation (continuum) and results in mode-locking stabilization. In the model, the positive feedback can occur by two ways: employing the ideal saturable absorber or by means of frequency shifted feedback (FSF) [25], [27]. Of course, the hybrid method combining both mechanisms is also possible. In the simulations all these options were studied. The simulation results illustrating the propagation of two pulses in the cavity with and without frequency-shifting are shown in Fig. 4. First, the scenario corresponding to the frequency shift being switched off is considered. In this case the generation of two initial pulses is maintained when the gain saturation energy stays within the range $70 \text{ pJ} < E_g < 125 \text{ pJ}$. Exceeding the maximum value leads to the development of instabilities. Figs. 4(a-c) show the results corresponding to the maximum value $E_g = 125 \text{ pJ}$. Fig 4(a) demonstrates the pulse arrangement after 6000 cavity roundtrips and the gain distribution $g(t)$ inducing the change in

the interpulse distance T_1, T_2 . The evolution of the interpulse distance difference $T_1 - T_2 = \Delta$ is extremely slow – after 6000 cavity roundtrips, the value of Δ changes by less than 1 ps (Fig. 4(c)), so the HML does not have enough time to be realized.

The frequency up-shift adding to the model significantly increases the nonlinear losses, so to maintain the generation of a pulse pair the gain saturation energy E_g should also be significantly increased and stays within the range $420 \text{ pJ} < E_g < 650 \text{ pJ}$. The value E_g can be optimized to achieve the fastest equalization of the pulse-to-pulse distances induced by the GDR. Figs. 4(c-e) demonstrate the results obtained when the gain saturation energy is closer to the lower limit of considered range $E_g = 450 \text{ pJ}$. In comparison with the previous case, the main result is that the periodical pulse arrangement corresponding to the HML in a laser with frequency shift is established quite fast: the value of Δ drops from the initial level $\Delta_0 = 6 \text{ ps}$ to 0 in less than 1000 roundtrips. Besides this one can note that the pulse generated in the hybrid mode-locked laser (“absorber” + “frequency shift”) possesses shorter duration ($\sim 3 \text{ ps}$ vs $\sim 5 \text{ ps}$ without frequency up-shift) and higher energy ($\sim 75 \text{ pJ}$ vs $\sim 30 \text{ pJ}$). The latest value is explained by higher gain saturation energy E_g . Elimination of the saturable absorber does not lead to fundamental changes in evolution Δ (dashed lines in Fig. 4(c)), confirming that the mode-locking and simultaneous stabilization of the pulse distribution can be successfully performed by the mechanism of frequency shift alone. In this case, the pulse energy even slightly increases due to the decrease of the nonlinear losses (Fig. 4(d)).

Additionally, we study the HML stability against noise perturbations in a hybrid mode-locked laser (pale red lines in Fig 4(c)).

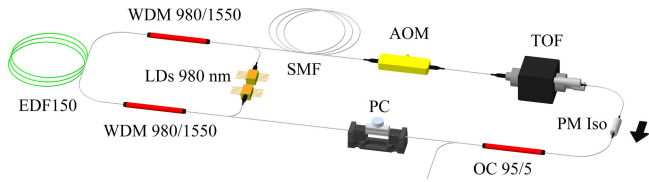


Fig. 5. Experimental setup. EDF – Er doped fiber, LDs – pump laser diodes, PC – polarization controller, AOM – acousto-optic modulator, TOF – tunable optical filter, PM Iso – polarization dependent isolator, OC – output coupler, SMF – passive single-mode fiber, WDM – wavelength-division multiplexer.

The noise was simulated by the simple way – a pair of cavity modes $\sim \exp(\pm 2\pi i t/T_R)$ with random phases and with the intensity of -15 dB with respect to the mean cavity intensity, which is excited randomly on average every 1000 roundtrips. The excited noise leads to random changes in pulse frequencies and distortions of their trajectories provoking the deviations from the uniform HML pulse arrangement. Due to the frequency shift, these fluctuations known as a timing jitter are quickly suppressed returning the pulses to the equilibrium positions with $\Delta = 0$.

Summarizing this paragraph, we can conclude that the simulations confirm the theoretical predictions. The soliton laser with an induced frequency shift and pulse repulsion implemented through the GDR approaches the HML state much faster than a similar laser without frequency shift. In the practical realization, it can be expected that the HML stability maintained through low-intensity pulse repulsion mechanisms (for example, GDR) is very limited. During a relatively long time of equidistant pulse arrangement in the laser cavity without frequency shift, the highly probable strong noise perturbations can lead to the jump in the interpulse distances and disturb the pulse position. As a result, the HML state of the laser either does not have time to be implemented or is extremely unstable, inevitably turning into chaotic pulse distribution in the cavity. At the same time, the frequency shift mechanism increasing the strength of pulse repulsion undoubtedly leads to better stability of the HML, since in this case, any fluctuation of the periodic pulse distribution is rapidly suppressed.

IV. EXPERIMENT

To experimentally verify the theoretical predictions described in previous sections, we design and build Er-doped fiber laser, which setup is shown in Fig. 5. During experiments, we compare two cavity designs with and without acousto-optic modulator (AOM) providing frequency shift. The fiber ring cavity consists of 0.85-m long erbium-doped fiber (EDF-150) as a gain medium with the dispersion $D = -48$ ps/(nm km) which is pumped by two CW laser pump diodes at 980 nm with a maximum pump power of 550 mW each. All passive fiber components of the scheme are made with standard telecom single-mode fiber SMF-28 ($D = 17$ ps/(nm km) at 1550 nm). Unidirectional laser emission is ensured by a fiber optical isolator. The output coupling of 5% generated light is carried out via an output coupler (95/5). The fundamental frequencies are $f_T = 11.03$ MHz for the

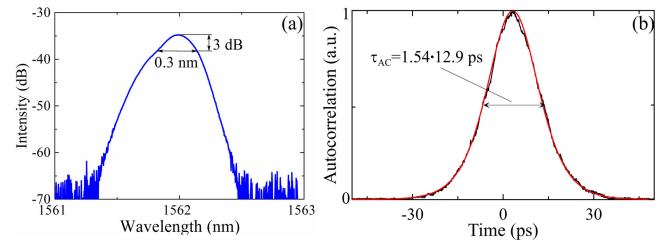


Fig. 6. The ring cavity laser with the frequency shifting. The measured optical spectrum (a) and autocorrelation trace (b) of the pulse in the HML regime at a repetition rate of 2.01 GHz. The red curve shows the sech^2 fitting.

cavity with AOM and $f_T = 12.04$ MHz without AOM. An intracavity acousto-optic modulator (AOM T-M080-0.4C2J-3-F2S) operates as a shifter with the frequency up-shift $\Delta\nu = 80$ MHz. An intracavity spectral band filtering is realized employing a tunable optical filter (TOF-1550-SM-L-10-NE) with 3 dB bandwidth ~ 1.2 nm. It allows tuning the central wavelength within the band of 1530–1570 nm. The output spectra of the laser are measured by an optical spectrum analyzer HP 70950B with 0.1 nm resolution. The RF spectrum analyzer coupled with detector MACOM D-8IR is used to monitor the RF signal. Autocorrelation traces are recorded by scanning autocorrelator FR103-WS.

According to the experimental observations the frequency-shifted laser exhibits mode-locked operation in a sufficiently wide filter-tuning range (from 1555 nm to 1565 nm). However, the best results are obtained when the central filter wavelength is fixed at $\lambda_0 = 1562$ nm. At this wavelength, the mode-locking at fundamental frequency occurs with appropriate polarization tuning at a low pump power of about 50 mW. By increasing the pump, the laser operation transits to the HML regime, wherein the pulse repetition rate grows almost proportionally to the pump power. At the fixed pump power, some additional tuning of the pulse repetition rate can be made by fine polarization adjustment. In this case, the maximum repetition rate of 2.01 GHz (182nd the cavity harmonic) is obtained at the pump power of about 800 mW while the output power is 1.0 mW, which corresponds to the output pulse energy of ~ 0.5 pJ. The optical spectrum and autocorrelation trace of the pulse are depicted in Fig. 6. The autocorrelation trace is well fitted to sech^2 -shape. The 3 dB pulse spectrum width is estimated as $\Delta\lambda_{FWHM} = 0.3$ nm, and the temporal full width at half-maximum (FWHM) of the pulse is $\Delta T_{FWHM} = 12.9$ ps. The time-bandwidth product is approximately 0.46, so the pulses can be considered as a nearly transform-limited soliton.

The pulse train stability is demonstrated by the RF spectra with different resolutions, which are shown in Fig. 7(a, b). For convenient comparison of different laser schemes, we present the experimental data at 1.059 GHz (96th cavity harmonic) obtained at 650 mW pump level. The large-scale RF spectrum recorded with a resolution of 20 MHz (inset in Fig. 7(a)) demonstrates the harmonics of the repetition rate with an insignificant additional modulation and slow variation of the peak intensity with the frequency. The RF spectrum with a resolution of 2 kHz (Fig. 7(a)) shows a sequence of super-mode noise peaks spaced apart by

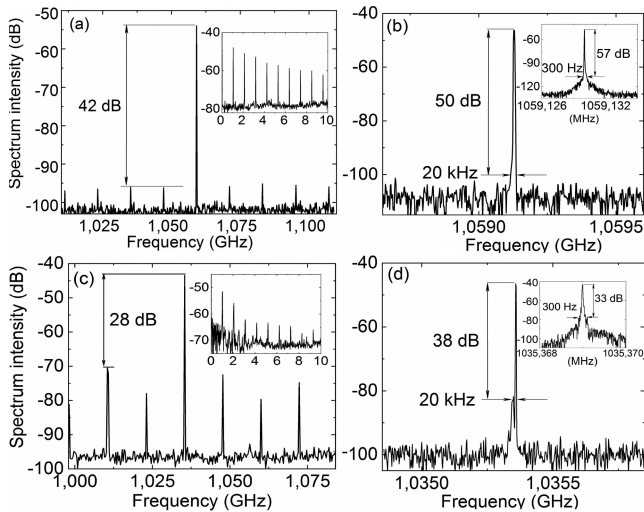


Fig. 7. The recorded RF spectra of the pulse trains obtained for (a, b) frequency-shifted laser with 1.059 GHz repetition rate and (c, d) for non-shifted laser with 1.035 GHz repetition rate. (a, c) resolution 200 kHz, inset – resolution 20 MHz, (b, d) resolution 2 kHz, inset – resolution 20 Hz.

a fundamental frequency f_T , that is the typical feature of HML lasers. The measured super-mode suppression level (SSL) of the pulse train is higher than 42 dB corresponding to the most stable HML lasers with NPR mode-locking [9]. All these signs match the robust harmonic pulse arrangement within the cavity. The value of timing jitter can be quantified based on the RF spectra data by using von der Linde method [32]. RF spectrum with resolution of $\Delta f_{res} = 20$ Hz (inset in Fig. 7(b)) shows that the signal to noise ratio (SNR), i.e the ratio of the maximum intensity of the spectral peak to the intensity of the noise band with the width of $\Delta f = 300$ Hz, is equal to $\Delta P = 57$ dB. For the ratio of rms jitter Δt to the pulse repetition rate $\Delta T = T/N$, where $T = 1/f_T$, and $N = 96$, we can obtain $\Delta t/\Delta T = (2\pi)^{-1} \cdot (\Delta P \cdot \Delta f/\Delta f_{res})^{1/2} \approx 0.087\%$. However, it is important for HML lasers to take into account the contribution from super-mode noise, which, under the assumption of uncorrelated noise, increases jitter by \sqrt{N} times [33]. Thus, for low-frequency jitter with the width $\Delta f = 300$ Hz we obtain $\Delta t \approx 7.5$ ps. Similarly, from RF spectrum with the resolution $\Delta f = 2$ kHz (Fig. 7(b)) for high-frequency timing jitter with the width $\Delta f = 20$ kHz we can obtain the value $\Delta t \approx 14.5$ ps. Exclusion of AOM from the experimental setup leads to slightly decrease in the cavity losses, but other characteristics remain almost unchanged (except the fundamental frequency that increases from 11.03 MHz to 12.04 MHz). To obtain a stable mode-locking at the fixed pump requires not only careful polarization adjustment but also tuning of the filter frequency. As a result, mode-locking occurs only at the center wavelength of the filter $\lambda_0 \approx 1557$ nm. In this case, the laser is mode-locked at the fundamental frequency at 40 mW of the pump power. The pump increase cause a drop off the mode-locked operation, however, at some fixed values of the pump power, it is possible to establish the HML by careful adjustment of the polarization controller. Eventually, the maximum repetition rate of the pulse train achieved at a pump power of about 600 mW is 1035 MHz (86th the cavity harmonic).

The further increase of the pump power results in breaking of the mode-locked operation. The parameters of the generated pulse are close to the pulse obtained in the frequency-shifted laser scheme. The 3 dB spectrum bandwidth is $\Delta\lambda_{FWHM} = 0.31$ nm, the temporal FWHM pulse width is $\Delta\tau_{FWHM} = 12.3$ ps, and the pulse shape is well fitted by sech^2 function. The main difference in the experimental results become obvious by comparing the RF spectra (Fig.7(c, d)). In contrast to the previous case, the large-scaled RF spectrum (inset in Fig. 7(c)) contains remarkable noise modulations and additional spikes demonstrating the imperfect HML. The medium-resolution spectrum (Fig. 7(c)) shows also the significantly lower SSL (~ 28 dB). The reduced SNR value (~ 33 dB to the noise with $\Delta f = 300$ Hz bandwidth), obtained from the RF spectrum with 20 Hz resolution, gives the possibility to estimate low-frequency timing jitter of the pulse train as equal to $\Delta t \approx 115$ ps. Similarly, from the RF spectrum with the resolution 2 kHz high-frequency timing jitter with the width $\Delta f = 20$ kHz, can be quantified as $\Delta t \approx 55$ ps that also noticeably superior to high-frequency timing jitter of the frequency shifted laser. Thus, the experiment demonstrates that the frequency shift contributes to the significant decrease of timing jitter and stabilization of HML in a ring soliton fiber laser.

V. CONCLUSION

Theoretical calculations based on the generalized NLS showed that multi-soliton dynamic system with interpulse repulsion through the GDR effect and frequency up-shift came to the equilibrium point much faster than a similar system without frequency shift. Physically, the acceleration of the system evolution to the equilibrium point is equivalent to increasing in repulsion strength or, in other words, deepening of “potential wells”, which lead to periodic pulse distribution in the cavity.

The numerical model of the ring soliton laser with interpulse repulsion induced by gain depletion and recovery agrees with the theoretical predictions. The frequency up-shift implemented into the model allowed reducing the time of the HML formation by orders of magnitude. Numerical simulations of HML arrangement also confirmed these conclusions after induced noise perturbations in the system. The simulations showed that the frequency shifting mechanism might be responsible both for mode-locking and for simultaneous stabilization of the periodic pulse distribution. It is important to note that the results obtained theoretically and numerically for the two pulses can be quite easily generalized for an arbitrary number of pulses propagating in the cavity [29].

Finally, the frequency-shifted HML ring fiber laser was experimentally realized and compared with a similar laser without frequency shift. The pulse parameters of two soliton lasers are close to each other, so we can assume that the mode-locking in both lasers was initiated by the same mechanism. The HML state achieved in both cases indicated the existence of pulse repulsion arising from some interaction mechanism. The GDR and acoustic interactions remain the main candidates for the role of the most intense interaction [29]; however, this issue requires additional research. It is important to note that the maximal pulse

repetition rates obtained in both cases (1 GHz and 2 GHz) did not differ drastically, so the interaction mechanism did not depend on the presence of frequency shift. However, there were several principal differences between the frequency-shifted laser and the laser mode-locked by NPR only. One was the limited wavelength range where non-shifted laser could be mode-locked by NPR only, at the same time a similar laser with frequency up-shift possessed higher nonlinear losses and it could be mode-locked in the extended wavelength range. The main differences between two cases concerned the stability of the generated pulse train to the noise-induced perturbations. In the laser configuration without frequency shift, the RF spectrum data indicated high fluctuations of the uniform pulse distribution, so the quality of the HML operation was rather poor. In its turn, both the low- and high-frequency timing jitter of the frequency-shifted laser were significantly smaller than the same characteristics for the non-shifted laser demonstrating quite stable periodic pulse arrangement within the cavity. Moreover, the stabilizing effect of the frequency shift is further confirmed by the fact that the low-frequency timing jitter of the frequency-shifted laser corresponding to a longer correlation time is substantially less than the high-frequency jitter. Thus, the experiment confirmed the theoretical predictions and the results of numerical simulation.

The main result of this study is the improved stability of high-repetition-rate pulse trains generated by the frequency up-shifted HML soliton laser. This outcome can enhance the physics of hybrid HML lasers and be extended to the laser cavities with saturable absorbers based on SESAM or carbon nanotubes. Undoubtedly, the results of this research can be interesting to a wide range of laser physics specialists engaged in different problems, from studying the nature of the laser pulses interaction to the generation of frequency combs and ultrahigh repetition rate pulse trains.

REFERENCES

- [1] S. A. Diddams, K. Vahala, and T. Udem, "Optical frequency combs: Coherently uniting the electromagnetic spectrum," *Science*, vol. 369, no. 6501, Jul. 2020, Art. no. eaay3676.
- [2] S. Droste *et al.*, "Optical frequency comb generation based on erbium fiber lasers," *Nanophotonics*, vol. 5, no. 2, pp. 196–213, Jun. 2016.
- [3] L. C. Sinclair *et al.*, "A compact optically coherent fiber frequency comb," *Rev. Sci. Instrum.*, vol. 86, no. 8, Aug. 2015, Art. no. 081301.
- [4] X. Liu and M. Pang, "Revealing the buildup dynamics of harmonic mode-locking states in ultrafast lasers," *Laser Photon. Rev.*, vol. 3, no. 9, Aug. 2019, Art. no. 1800333.
- [5] C. S. Jun *et al.*, "Toward higher-order passive harmonic mode-locking of a soliton fiber laser," *Opt. Lett.*, vol. 37, no. 11, pp. 1862–1864, Jun. 2012.
- [6] Z. C. Luo *et al.*, "2 GHz passively harmonic mode-locked fiber laser by a microfiber-based topological insulator saturable absorber," *Opt. Lett.*, vol. 38, no. 24, pp. 5212–5215, Dec. 2013.
- [7] M. Chernysheva *et al.*, "Carbon nanotubes for ultrafast fibre lasers," *Nanophotonics*, vol. 6, no. 1, pp. 1–30, Jun. 2017.
- [8] H. Kalaycıoğlu, P. Elahi, Ö. Akçaalan, and F. Ö. Ilday, "High-repetition-rate ultrafast fiber lasers for material processing," *IEEE J. Sel. Top. Quantum Elect.*, vol. 24, no. 3, pp. 1–12, May/June 2018.
- [9] C. Lecaplain and P. Grelu, "Multi-gigahertz repetition-rate-selectable passive harmonic mode locking of a fiber laser," *Opt. Exp.*, vol. 21, no. 9, pp. 10897–10902, May 2013.
- [10] A. I. Trikshev *et al.*, "Passive harmonic mode-locking in an erbium-doped fibre laser," *Quantum Elect.*, vol. 48, no. 12, pp. 1109–1112, Dec. 2018.
- [11] Q. Huang, Z. Huang, M. A. Aramii, A. Rozhin, and C. Mou, "2.4 GHz L-band passively harmonic mode locked Er-doped fiber laser based on carbon nanotubes film," *IEEE Photon. Technol. Lett.*, vol. 32, no. 2, pp. 121–124, Jan. 2020.
- [12] G. Sobon, J. Sotor, and K. M. Abramski, "Passive harmonic mode-locking in Er-doped fiber laser based on graphene saturable absorber with repetition rates scalable to 2.22 GHz," *Appl. Phys. Lett.*, vol. 100, no. 16, Apr. 2012, Art. no. 161109.
- [13] R. S. Fodil *et al.*, "Adjustable high-repetition-rate pulse trains in a passively-mode-locked fiber laser," *Phys. Rev. A*, vol. 94, no. 1, Jan. 2016, Art. no. 013813.
- [14] D. Mao *et al.*, "Flexible high-repetition-rate ultrafast fiber laser," *Sci. Rep.*, vol. 3, no. 1, pp. 1–5, Nov. 2013.
- [15] D. A. Korobko, A. A. Fotiadi, and I. O. Zolotovskii, "Mode-locking evolution in ring fiber lasers with tunable repetition rate," *Opt. Exp.*, vol. 25, no. 18, p. 21180–21190, Aug. 2017.
- [16] A. B. Grudinin and S. Gray, "Passive harmonic mode locking in soliton fiber lasers," *J. Opt. Soc. Amer. B*, vol. 14, no. 1, pp. 144–154, Jan. 1997.
- [17] D. A. Korobko, O. G. Okhotnikov, and I. O. Zolotovskii, "Long-range soliton interactions through gain-absorption depletion and recovery," *Opt. Lett.*, vol. 40, no. 12, pp. 2862–2865, Jun. 2015.
- [18] G. Semaan *et al.*, "Study of a harmonic mode lock stability under external continuous-wave injection," *Opt. Commun.*, vol. 387, pp. 65–69, Mar. 2017.
- [19] A. N. Piliptsckii, E. A. Golovchenko, and C. R. Menyuk, "Acoustic effect in passively mode-locked fiber ring lasers," *Opt. Lett.*, vol. 20, no. 8, pp. 907–909, Apr. 1995.
- [20] S. Gray, "Femtosecond harmonically mode-locked fiber laser with time jitter below 1 ps," *Opt. Lett.*, vol. 20, no. 2, pp. 189–191, Jan. 1995.
- [21] T. Noronen, O. Okhotnikov, and R. Gumenyuk, "Electronically tunable thulium-holmium mode-locked fiber laser for the 1700–1800 nm wavelength band," *Opt. Exp.*, vol. 24, no. 13, pp. 14703–14708, Jun. 2016.
- [22] R. V. Gumenyuk, D. A. Korobko, and I. O. Zolotovskii, "Stabilization of passive harmonic mode locking in a fiber ring laser," *Opt. Lett.*, vol. 45, no. 1, pp. 184–187, Jan. 2020.
- [23] D. A. Korobko *et al.*, "Harmonic mode-locking fiber ring laser with a pulse repetition rate up to 12 GHz," *Opt. Laser Technol.*, vol. 133, pp. 106526–106530, Jan. 2021.
- [24] S. Bonnet *et al.*, "Dynamics and self-modelocking of a titanium-sapphire laser with intracavity frequency shifted feedback," *Opt. Commun.*, vol. 123, no. 4–6, pp. 790–800, Feb. 1996.
- [25] Y. Kodama and S. Wabnitz, "Analysis of soliton stability and interactions with sliding filters," *Opt. Lett.*, vol. 19, no. 3, pp. 162–164, Feb. 1994.
- [26] J. M. Sousa and O. G. Okhotnikov, "Short pulse generation and control in Er-doped frequency-shifted-feedback fibre lasers," *Opt. Commun.*, vol. 183, no. 1–4, pp. 227–241, Sep. 2000.
- [27] C. M. D. Sterke and M. J. Steel, "Simple model for pulse formation in lasers with a frequency-shifting element and nonlinearity," *Opt. Commun.*, vol. 117, no. 5/6, pp. 469–474, Jun. 1995.
- [28] D. Y. Tang *et al.*, "Soliton interaction in a fiber ring laser," *Phys. Rev. E*, vol. 72, no. 1, Jul. 2005, Art. no. 016616.
- [29] J. N. Kutz, B. C. Collings, K. Bergman, and W. H. Knox, "Stabilized pulse spacing in soliton lasers due to gain depletion and recovery," *IEEE J. Quantum Elect.*, vol. 34, no. 9, pp. 1749–1757, Sep. 1998.
- [30] A. Komarov, H. Leblond, and F. Sanchez, "Theoretical analysis of the operating regime of a passively-mode-locked fiber laser through nonlinear polarization rotation," *Phys. Rev. A*, vol. 72, no. 6, Dec. 2005, Art. no. 063811.
- [31] C.-J. Chen, P. K. A. Wai, and C. R. Menyuk, "Soliton fiber ring laser," *Opt. Lett.*, vol. 17, no. 6, pp. 417–419, Mar. 1992.
- [32] D. V. D. Linde, "Characterization of the noise in continuously operating mode-locked lasers," *Appl. Phys. B*, vol. 39, no. 4, pp. 201–217, Apr. 1986.
- [33] F. Rana *et al.*, "Characterization of the noise and correlations in harmonically mode-locked lasers," *J. Opt. Soc. Amer. B*, vol. 19, no. 11, pp. 2609–2621, Nov. 2002.